Available online at www.sciencedirect.com
ScienceDirect
Engineering Fracture Mechanics 75 (2008) 3121–3130
Engineering Fracture Mechanics
www.elsevier.com/locate/engfracmech

Elastic anisotropy effect on indentation-induced thin film interfacial delamination

B. Yang [a,*], A.A. Volinsky [b]

[a] Department of Mechanical and Aerospace Engineering, Florida Institute of Technology, Melbourne, FL 32901, United States
[b] Department of Mechanical Engineering, University of South Florida, Tampa, FL 33620, United States

Received 21 August 2007; received in revised form 3 December 2007; accepted 13 December 2007
Available online 25 December 2007

Abstract

Effect of elastic anisotropy on indentation-induced thin film interfacial delamination, especially, at the initiation and early growth stage, is examined. The indentation load is modeled as a constant pressure over an expanding semi-spherical cavity. The delamination process is approached by a cohesive zone model. The rest of the problem is formulated within the general anisotropic elasticity theory, and solved numerically by the boundary element method employing a special Green's function for multilayers. The material system of a Cu(0 0 1) film on a Si(0 0 1) substrate is studied as an example. The interfacial damage initiation and crack development under indentation are captured in the simulation. By comparing the predictions with the materials being modeled as isotropic and as anisotropic (of the cubic symmetry as they are), it is shown that the elastic anisotropy of the copper film plays a significant role in determining the delamination pattern. In the isotropic model, the delamination crack fronts are circular reflecting the problem axisymmetry. In contrast, crack fronts are square with rounded corners in the anisotropic case. This significant difference necessitates a three-dimensional anisotropic stress analysis of the indentation-induced delamination of strongly anisotropic films.

Keywords: Adhesion; Anisotropic elasticity; Boundary element method; Cohesive zone model; Delamination; Expanding cavity model; Fracture mechanics; Indentation; Thin films

1. Introduction

Indentation test is one of the promising techniques for measuring thin film adhesion energy [13,17,1,19,10]. Pressed into a film, an indenter induces large lateral stress by repelling surrounding material aside, which in turn may suffice to drive the film to delaminate from the substrate. Success of the indentation technique relies on accurate characterization of the indentation load and the delamination crack size. If the film is transparent, the delamination crack size can be measured in situ under an optical microscope [17,5]. Otherwise, it is measured ex situ after the film delaminates and buckles [14,19].

* Corresponding author. Tel.: +1 321 674 7713; fax: +1 321 674 8813.
E-mail address: boyang@fit.edu (B. Yang).

0013-7944/$ - see front matter © 2007 Elsevier Ltd. All rights reserved.
doi:10.1016/j.engfracmech.2007.12.008

A full model of plasticity and crack growth is necessary to accurately predict the process of film delamination under indentation. However, the corresponding computational task is prohibitively elaborate given the current computer technology. Therefore, simplified but elegant models have been developed to characterize the indentation loading in certain extreme cases. For the case of a film undergoing extensive plastic deformation on a rigid substrate, Marshall and Evans model [13] has been developed and widely adopted. It assumes that the plastic zone under an indenter takes a cylindrical shape and that the indentation volume is entirely translated into lateral elastic displacement to load the delamination crack. In another case of a small plastic zone under indentation (relative to the film thickness), the expanding cavity model can be used [11]. The plastic zone shape is assumed to be semi-spherical, and a constant pressure (a fraction of the film yield strength) is applied at the plastic zone boundary to load the delamination crack. The plastic zone size is determined from the volume conservation, i.e., the volume swept by the elastic–plastic boundary through its displacement is equated to the indentation volume. These two models are essentially identical, assuming that the entire indentation volume is translated into elastic loading, with the only difference in the shape of the elastic–plastic boundary. While the former is applicable to strong interfaces on a rigid substrate, the latter is applicable to relatively weak interfaces or thick films.

In previous studies, an axi-symmetric two-dimensional (2D) model has been adopted [13,1]. It implies that the film and the substrate materials are both isotropic or at least transversely isotropic normal to the film. It also implies that the delamination front is circular. The present work aims to relax the axisymmetry assumption, and carry out a 3D simulation of the delamination process in an anisotropic film and substrate material system. Based on the simulation, the effect of the elastic anisotropy on the delamination pattern is examined. The material system of a Cu(0 0 1) film on a Si(0 0 1) substrate is studied as an example. It is shown that the elastic anisotropy of copper makes a significant difference in the delamination pattern. In contrast, the relatively weak anisotropy of silicon makes little difference. The simulations have captured the delamination damage initiation and further crack development processes under indentation.

The rest of the paper is organized as follows. In Section 2, the expanding cavity model of indentation is summarized [11], followed by the cohesive zone model of delamination damage and crack development [2,7]. In Section 3, the special boundary element method for multilayers [22,23], adopted to solve the problem, is summarized. Since the Green's function for multilayers used satisfies the interfacial continuity and traction-free surface conditions [25,30], only the delamination crack and the indentation semi-spherical elastic–plastic boundary where pressure is applied need to be numerically discretized. This enabled us to efficiently and accurately conduct an extensive parametric study of the progressive delamination problem under indentation. In Section 4, numerical results are discussed. In Section 5, conclusions are drawn.

2. Problem formulation

Consider an indentation of a thin film of thickness t on a semi-infinite substrate with a rigid indenter, schematically shown in Fig. 1a. When the indenter is pressed into the film with a force P_I, it causes a permanent impression of volume V_I. The material originally residing in the impression volume is pushed away in all possible directions, including a significant fraction that induces elevated lateral stresses to load the film-substrate interface. This loading due to finite plasticity is much larger than the elastic portion. These lateral stresses may

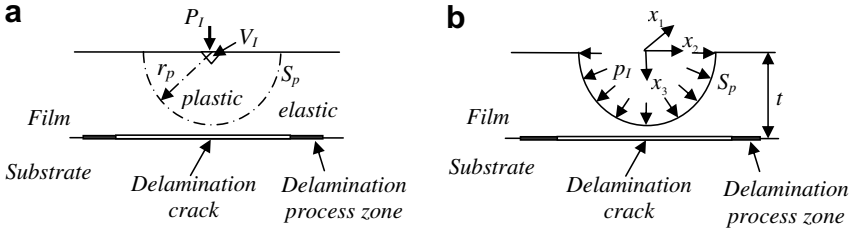

Fig. 1. (a) Schematics showing delamination damage and crack in a thin-film-on-substrate structure under indentation; (b) solid to be simulated that excludes the indentation plastic zone.

be high enough to cause the film to delaminate from the substrate. During this process, there are two focal points of interest: the indentation plastic zone, and the delamination crack. Of our greater interest is the latter; thus, an approximate expanding cavity model is adopted to characterize the indentation loading. The delamination process is approached by the cohesive zone model in order to predict an arbitrary shape of the delamination front. With the cohesive zone model, the delamination process is conveniently captured as a natural debonding process of the film from the substrate, described by a cohesive force law. The capability of predicting an arbitrary delamination front is necessary in order to examine the effect of film and/or substrate elastic anisotropy on the delamination pattern of our interest in the present work.

The expanding cavity model, as shown in Fig. 1b, assumes a semi-spherical shape of an elastic–plastic boundary underneath an indenter, and a uniform pressure transmitted through the elastic–plastic boundary to load a delamination crack. The size of the plastic zone is determined by equating the volume swept by the elastic–plastic boundary through its displacement to the indentation volume. It is implied that the model can be inaccurate if significant pile-up occurs around the indenter. Another possible source of inaccuracy is the assumption of uniform pressure along the elastic–plastic boundary. It is clear that the pressure is two thirds of the film yield strength away from the free surface. Near the free surface, the pressure is in contrast equal to the film yield strength [11]. Since the delamination crack is loaded by the pressure aligned in the lateral directions, it is taken to be equal to the film yield strength. The model application is limited to a small plastic zone size, before it reaches the interface in order to avoid further complication/inaccuracy.

The configuration excluding the indentation plastic zone that will be numerically modeled later is shown in Fig. 1b. The total indentation force P_I and the indentation volume V_I can be derived from the stress and displacement fields along the elastic–plastic boundary S_p:

$$P_I = \int_{S_p} p_I n_3 \, dS, \tag{1}$$

$$V_I = \int_{S_p} u_n \, dS, \tag{2}$$

where p_I is the pressure, n_3 is the third component of the outward normal $\boldsymbol{n}$, and u_n is the normal component of the displacement, respectively, over S_p. The Cartesian coordinate system with the third axis perpendicular to the film surface is established. The cubic root of V_I has linear dependence on the indentation depth, and the proportionality coefficient depends on the indenter tip geometry. For the details of the stress field in the plastic zone, one may refer to the textbook of Johnson [11] in the case of elastic-perfectly plastic materials and to more recent publications of Gao [9] and Gao et al. [8] in the case of appreciable hardening and local effects.

The cohesive zone model is well suited for simulating arbitrary crack front development during the indentation process. Originally developed for modeling plastic deformation at a crack tip (i.e., a strip yield model) [7] and atomic decohesion [2], the cohesive zone model has been advanced to take into account loading rate dependence [3,21], unloading [16,26], fatigue loading [24,15], etc. An excellent review of the cohesive zone model and its applications can be found in Yang and Cox [29]. In the present application, the delamination crack is entirely closed, and loaded only in the shear mode. Since the tractions on opposite crack faces are equal in magnitude and are opposite in direction, either one can be used to represent the loading of the cohesive zone material, and is related to the corresponding deformation, i.e., the crack displacement jump $[\boldsymbol{u}]$. The cohesive zone thickness effect is neglected. The traction $\boldsymbol{p}$ on one side of the crack is related to $[\boldsymbol{u}]$ as

$$p = k[u], \tag{3}$$

where k is the cohesive zone stiffness, assumed to be a scalar, as in a line-spring model. The stiffness k softens with a damage parameter w_d, taken to be the maximum magnitude of the displacement jump that the cohesive zone material has ever experienced:

$$k = \frac{p_d}{w_d}, \tag{4}$$

where p_d is a function of w_d, representing the damage locus. The damage locus is taken to be a constant, truncated at a critical damage parameter w_f, as shown in Fig. 2. The damage process is irreversible. When the cohesive zone material is loaded monotonically, it will eventually reach the damage locus and subsequently

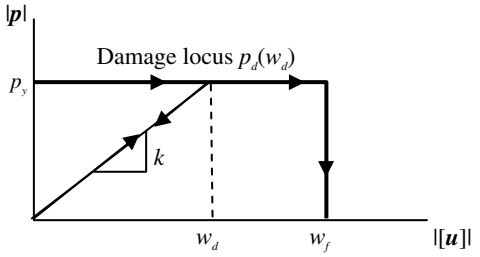

Fig. 2. Cohesive damage locus of a constant damage-flow stress p_y, truncated at a critical failure parameter w_f.

follow it with further damage progression. When unloaded at a certain point of the damage locus, the damage parameter w_d is held constant, and the state linearly recedes by the corresponding slope k, as shown in Fig. 2. When reloaded, it follows the same path of slope k back to the damage locus and subsequently follows the damage locus until complete failure at w_f. The consideration of unloading behavior is necessary in order to simulate an arbitrary process of film interfacial delamination in three dimensions.

After excluding the indentation plastic zone and applying the cohesive zone model to the delamination process, the rest of the problem is to model the film and the substrate deformation applying the anisotropic elasticity theory [18]. The equilibrium condition requires that

$$\sigma_{ij,j} = 0, \tag{5}$$

where $\boldsymbol{\sigma}$ is the stress tensor, the prime in the subscript indicates the partial differentiation with respect to the axis that follows, and the repeated subscript indices imply the Einstein convention of summation over their ranges. The constitutive law is given by

$$\sigma_{ij} = C_{ijkl} u_{k,l}, \tag{6}$$

where $\boldsymbol{C}$ is the elastic stiffness matrix. The film surface is traction-free. Pressure equal to the yield strength of the film is imposed at the boundary of the indentation plastic zone. The film-substrate interface is initially perfectly bonded, and subjected to progressive delamination damage and cracking under indentation by the above cohesive damage law. The remote radiation condition, i.e., zero displacement at infinite distance, is enforced.

3. Boundary element method for multilayers

Applying Green's function for multilayers [25,30], the displacement field in the solid as described in the previous section is expressed as

$$c_{ij} u_j(\boldsymbol{X}) = \int_{S_p} (u^*_{ij}(\boldsymbol{X}, x) p_j(\boldsymbol{x}) - p^*_{ij}(\boldsymbol{X}, x) u_j(\boldsymbol{x})) \mathrm{d}S + \int_{S_c} p^*_{ij}(\boldsymbol{X}, x) [u_j(\boldsymbol{x})] \mathrm{d}S, \tag{7}$$

where S_p is the semi-spherical loading boundary, i.e., the boundary of indentation plastic zone, S_c is one side of the crack, and $\boldsymbol{c}$ is a constant, depending on the location of $\boldsymbol{X}$. If $\boldsymbol{X}$ is located inside the solid, $\boldsymbol{c}$ is given by the identity matrix (i.e., the Kronecker delta function δ_{ij}). If $\boldsymbol{X}$ is located on a smooth boundary, it is given by one half of the identity matrix. Green's functions $\boldsymbol{u}^*$ and $\boldsymbol{p}^*$, respectively, represent the displacement and the traction at $\boldsymbol{x}$ induced by a unit point force applied at $\boldsymbol{X}$ in the system of perfectly bonded film and substrate and a free surface. Note that the above integral equation involves only the altered boundary and the crack.

Taking derivatives of both sides of Eq. (7) with respect to $\boldsymbol{X}$ and applying Eq. (6) (i.e., the constitutive law), the integral equation of stress can be derived. If $\boldsymbol{X}$ is a boundary point, multiplying both sides of the derived integral equation of stress by the outward normal $\boldsymbol{n}$ at $\boldsymbol{X}$ yields the integral equation of traction. It is given by

$$p_i(\boldsymbol{X}) = \int_{S_p} (U^*_{ij}(\boldsymbol{X}, x) p_j(\boldsymbol{x}) - P^*_{ij}(\boldsymbol{X}, x) u_j(\boldsymbol{x})) \mathrm{d}S + \int_{S_c} P^*_{ij}(\boldsymbol{X}, x) [u_j(\boldsymbol{x})] \mathrm{d}S, \tag{8}$$

where $\boldsymbol{U}^*$ and $\boldsymbol{P}^*$ are combinations of $\boldsymbol{u}^*$ and $\boldsymbol{p}^*$ derivatives, respectively.

Eqs. (7) and (8) can be applied to develop an efficient and accurate boundary element method to solve the above formulated problem. Eq. (7) is applied to the boundary where the indentation pressure is applied, whilst Eq. (8) is applied to the crack. The loading boundary and the crack are discretized into constant elements. Substituting the approximated fields into Eqs. (7) and (8) yields a system of algebraic equations:

$$u_i^m = \sum_{n\in S_p}(g_{ij}^{mn}p_j^n + h_{ij}^{mn}u_j^n) + \sum_{n\in S_c} h_{ij}^{mn}[u_j^n], \tag{9}$$

$$p_i^m = \sum_{n\in S_p}(G_{ij}^{mn}p_j^n + H_{ij}^{mn}u_j^n) + \sum_{n\in S_c} H_{ij}^{mn}[u_j^n], \tag{10}$$

where the coefficients, $\boldsymbol{g}$, $\boldsymbol{h}$, $\boldsymbol{G}$ and $\boldsymbol{H}$ are integrals of Green's functions over an element, and the superscript indicates a node. The overall computational efficiency of the boundary element method is largely determined by the evaluation efficiency of these coefficients. A semi-analytical method has been recently developed to compute these integrals efficiently and accurately [28], which is adopted in the present study.

Given the pressure over the indentation loading boundary S_p and the cohesive force law governing the delamination process, the above system of algebraic equations can be solved numerically to obtain the displacement along the loading boundary and the displacement jump across the crack. The iterative scheme of successive over-relaxation, which has been successfully applied to solve similar problems [27,22,23], is adopted to solve the present problem. For the sake of brevity, it is not described here.

4. Results and analysis

The analyzed material system consists of a Cu(1 0 0) film on a Si(0 0 1) substrate. In order to demonstrate the effect of elastic anisotropy on the indentation-induced interfacial delamination, simulations are run with the materials being modeled first as isotropic and then as anisotropic (of the cubic symmetry as they are). The elastic constants of the two models are given in Tables 1 and 2, respectively. The anisotropic elastic constants of the copper and the silicon were taken from Cleri and Rosato [4] and Levinshtein et al. [12], respectively. Meanwhile, the isotropic elastic constants of both materials were taken from Dolbow and Gosz [6]. Zener's anisotropy index is defined as $\alpha = (2C_{66})/(C_{11} - C_{12})$. It is equal to one if the material is fully isotropic. Deviation from one indicates anisotropy, where greater deviation means stronger anisotropy. The anisotropy index is 3.22 for copper, and 1.56 for silicon. Therefore, copper exhibits stronger anisotropy than silicon.

The pressure imposed upon the elastic–plastic boundary is taken to be the yield strength of the copper film, equal to 100 MPa [6,20]. The delamination damage-flow stress p_y is taken to be 4 MPa, and the failure crack displacement jump w_f is taken to be $10^{-4}\cdot t$, where t is the film thickness. Thus, the film adhesion energy in the units of Joule is $400\cdot t$, where t is in meters. For example, if the film is 1 mm thick, the adhesion energy is 0.4 J. In the rest of text, including figures, all of the quantities of the length dimension are normalized by t, and all of the stress quantities are normalized by $E_0 = 1$ GPa. Note that the interfacial properties are chosen such that

Table 1
Elastic constants for copper and silicon in the isotropic model

	Young's modulus (GPa)	Poisson ratio
Copper	128	0.36
Silicon	165	0.22

Table 2
Elastic constants for copper and silicon in the anisotropic (cubic) model

	C_{11} (GPa)	C_{12} (GPa)	C_{44} (GPa)
Copper	176	125	82
Silicon	165	63.9	79.6

the cohesive zone size can be resolved accurately with the currently available computer power. Consequently, the following calculation may be inapplicable to a very thin film of thickness below one micron.

For the isotropic case, a set of simulations with various radii r_p of the indentation plastic zone S_p was carried out. Since the loading over this semi-spherical boundary is axi-symmetric about the x_3-axis, the induced stress field and hence the delamination pattern along the film-substrate interface is expected to be axi-symmetric about the normal direction. During the simulations, the total indentation force P_I and the indentation volume V_I are computed using Eqs. (1) and (2), respectively. Variations of the normalized indentation force $P_I/(E_0t^2)$ and the cubic root of the indentation volume $\sqrt[3]{V_I}/t$ with respect to r_p/t are plotted in Fig. 3. Four snapshots of the tangential traction ($\tau = \sqrt{p_1^2 + p_2^2}$) contour over the interface are plotted in Fig. 4. The normal traction component, i.e., pressure normal to the interface, does not contribute to the delamination process. A spider-web mesh of seven radial divisions per unit length and forty eight circumferential divisions was used as the potential zone of interfacial delamination damage and cracking. This mesh and the mesh used for the

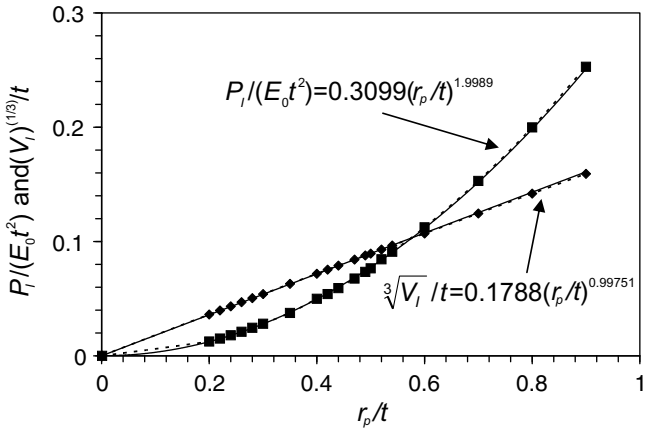

Fig. 3. Variation of normalized indentation force $P_I/(E_0t^2)$ and normalized cubic root of indentation volume $\sqrt[3]{V_I}/t$ with indentation plastic zone radius r_p/t. Also shown are the power-law curve fitting equations for the two data sets in the case of isotropic material model.

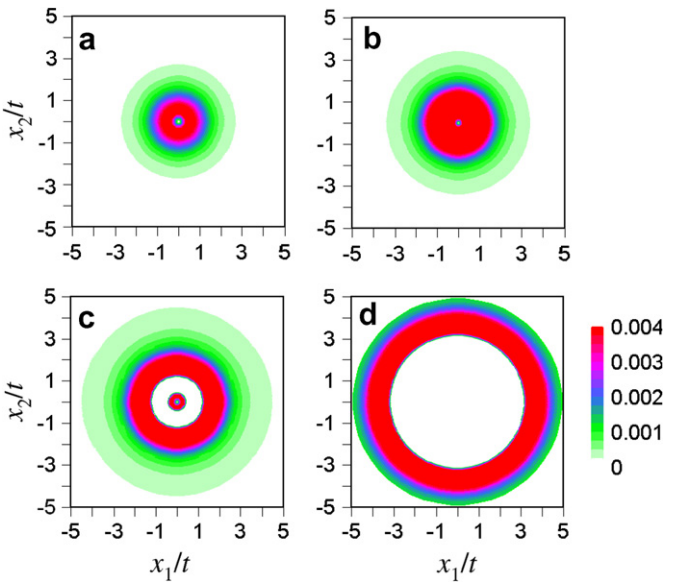

Fig. 4. Contour plots of tangential traction (GPa) along the interface at various values of r_p/t: (a) 0.3; (b) 0.4; (c) 0.5; (d) 0.8, in the case of isotropic material model. All the figures share the same scale bar as given in (d).

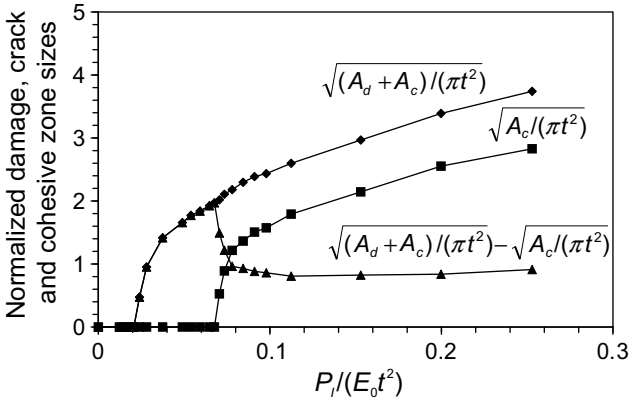

Fig. 5. Variation of normalized damage radius $\sqrt{(A_d + A_c)/\pi t^2}$, crack radius $\sqrt{A_c/\pi t^2}$, and cohesive zone depth $\sqrt{(A_d + A_c)/\pi t^2} - \sqrt{A_c/\pi t^2}$ with normalized indentation force $P_I/(E_0 t^2)$ in the case of isotropic material model.

semi-spherical loading boundary S_p were both checked to be adequately dense to provide accurate solution to the problem. The red[1] (dark) color indicates the delamination process zone. The white (bright) color indicates the location of trivial tangential traction. These figures clearly show the process of delamination damage initiation, crack initiation, and their further extension in both inward and outward radial directions. Furthermore, the cohesive damage and crack areas A_d and A_c are calculated. Their normalized variants, $\sqrt{A_c/(\pi t^2)}$, $\sqrt{(A_d + A_c)/(\pi t^2)}$, and $\sqrt{(A_d + A_c)/(\pi t^2)} - \sqrt{A_c/(\pi t^2)}$, indicating the average damage and crack radii and the average cohesive zone depth, respectively, are plotted as functions of normalized indentation force $P_I/(E_0 t^2)$ in Fig. 6.

A power-law curve fitting to the numerical data in Fig. 3 reveals that the cubic root of indentation volume V_I is proportional to r_p and that the total indentation force P_I is a quadratic function of r_p, which is consistent with the analytical solution of Johnson [11]. It is evident that the present formulation is valid and that the mesh used is adequate. Note that the linear dependence of $\sqrt[3]{V_I}$ and quadratic dependence of P_I on r_p are identified over the entire process of no cracking in the beginning to later significant delamination damage. This is expected because the delamination crack is always closed (before buckling of delaminated film) and because the indentation behavior is mainly dependent on the deformation in the normal direction to the film surface.

It can be seen from Fig. 4 that the delamination damage initiates at a certain distance from the middle symmetry point where the interfacial shear stress is the maximum and eventually reaches the interfacial strength, p_y. When the indentation progresses with increasing P_I, the damage extends in both inward and outward radial directions. Upon the preceding damage saturation, a crack is initiated (roughly at the same location of damage initiation), and extends following the damage fronts. The inner ligament eventually diminishes, meanwhile the outer crack and damage fronts continue to advance. This process of damage and crack development is quantitatively shown through the evolution of crack and damage areas in Fig. 5. After the ligament diminishes, $\sqrt{A_c/\pi}$ and $\sqrt{(A_d + A_c)/\pi}$ indicate the radii of the crack and damage fronts, and $\sqrt{(A_d + A_c)/\pi} - \sqrt{A_c/\pi}$ indicates the cohesive zone size. It can be seen that the damage evolution including its initiation and propagation is a gradual process. In contrast, the crack initiation is a jump-like event. Quickly after the initiation, the crack extends in steady state, indicated by a constant cohesive zone size. Here, we did not consider film bulking effects, so the crack length is assumed to be always smaller than the critical bulking length.

Another set of simulations was carried out, with the materials modeled as anisotropic. The numerical parameters were all the same as above except the material model. Thus, any difference in the predictions must be attributed to the effect of elastic anisotropy of the film and the substrate. Similar sets of results as above were obtained. Since the overall indentation behavior in the case of anisotropic material model is found to be virtually the same as above (although the constants of these two isotropic and anisotropic material models

[1] For interpretation of color in Figs. 4 and 6, the reader is referred to the web version of this article.

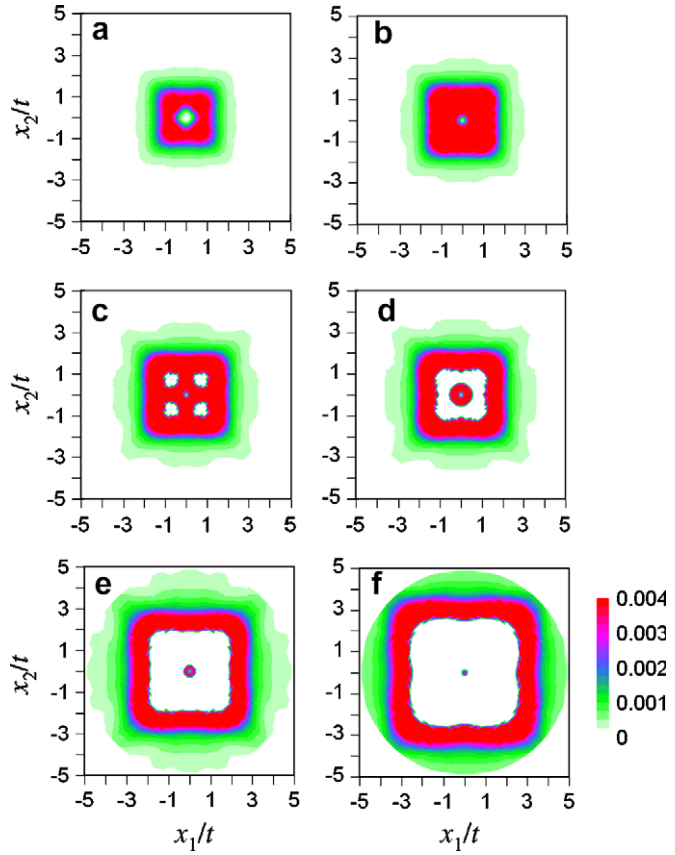

Fig. 6. Contour plots of normalized tangential traction (GPa) on the interface at various values of r_p/t: (a) 0.3; (b) 0.4; (c) 0.48; (d) 0.5; (e) 0.7; (f) 0.9, in the case of anisotropic material model. All the figures share the same scale bar as given in (f).

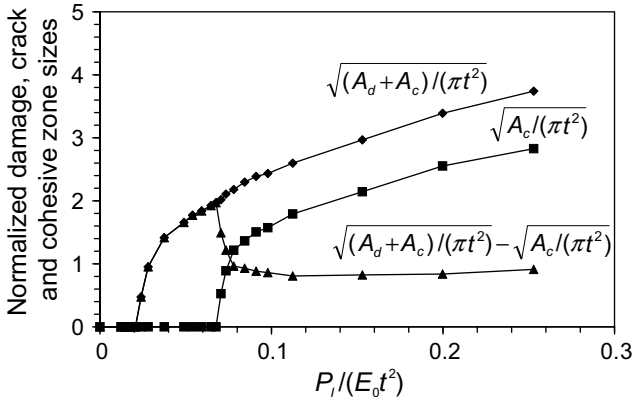

Fig. 7. Variation of normalized damage radius $\sqrt{(A_d + A_c)/\pi t^2}$, crack radius $\sqrt{A_c/\pi t^2}$, and cohesive zone depth $\sqrt{(A_d + A_c)/\pi t^2} - \sqrt{A_c/\pi t^2}$ with normalized indentation force $P_l/(E_0 t^2)$ in the case of anisotropic material model.

in Tables 1 and 2 were taken from different references), the plot similar to Fig. 3 is omitted. The comparable results to those in Figs. 4 and 5 are plotted in Figs. 6 and 7.

Almost the same qualitative discussion can be made about the loading and the delamination processes in the case of anisotropic material model as in the previous case of isotropic material model. However, a striking

difference is observed in the shape of the delamination damage and crack fronts being square with rounded corners compared to the circular shape attaining to the axi-symmetry in the previous isotropic case. The only possible explanation to this result is the material elastic anisotropy that has been taken into account. This strong deviation of the delamination front from the circular shape needs to be accounted for when interpreting experimental results in such material systems. Besides the significant effect of materials elastic anisotropy on delamination pattern, it is also seen that both damage and crack initiations are gradual, unlike discontinuous in the isotropic case.

Finally, further simulations were run with the copper film and the silicon substrate modeled as either isotropic or anisotropic. When the copper film is modeled as isotropic and the silicon substrate as anisotropic, the delamination front is circular. However, when the copper film is modeled as anisotropic and the silicon substrate as isotropic, it is square with rounded corners. This suggests that it is not the elastic anisotropy of the silicon substrate but that of the copper film that transforms the delamination pattern. Recall that the anisotropy index of the copper film is 3.22, compared to 1.56 for the silicon substrate.

5. Conclusions

A comparative computational study of the indentation-induced delamination process of thin films with and without elastic anisotropy has been carried out. The indentation load was treated by the expanding cavity model. The delamination process was treated by the cohesive zone model so that an arbitrary delamination front can be conveniently predicted. The main conclusion of this study is that in the case of a Cu(0 0 1) film on a Si(0 0 1) substrate, the elastic anisotropy plays a significant role in determining the delamination pattern. This is evidenced by very different predictions of a square delamination front with rounded corners in the anisotropic material model and a circular delamination front in the isotropic material model. The whole process of delamination damage and crack development at a film-substrate interface under indentation was captured. This study employing the semi-spherical cavity model is limited to the cases of relatively small indentation plastic zone compared to the film thickness, thus relatively weakly bonded interfaces. The present extensive parametric study was carried out by applying an efficient and accurate boundary element method employing the special Green's function for multilayers. Because Green's function satisfies the interfacial continuity and traction-free surface condition, the numerical discretization was only performed along the semi-spherical loading boundary and one side of the delamination crack.

Acknowledgement

This work is supported by the National Science Foundation (CMMI-0600266 and CMMI-0600231), the Division of Civil, Mechanical and Manufacturing Innovation. BY also acknowledges summer support from the National Institute of Standards and Technology that initiated this study. AV acknowledges the NSF IREE supplement support for the CMMI-0600231 Grant.

References

[1] Abdul-Baqi A, Van der Giessen E. Indentation-induced interface delamination of a strong film on a ductile substrate. Thin Solid Films 2001;381:143–54.
[2] Barenblatt GI. The mathematical theory of equilibrium cracks in brittle fracture. Adv Appl Mech, vol. VII. Academic Press; 1962. p. 55–129.
[3] Bazant ZP, Li Y-N. Cohesive crack model with rate-dependent opening and viscoelasticity: I. Mathematical model and scaling. Int J Fract 1997;86:247–65.
[4] Cleri F, Rosato V. Tight-binding potentials for transition metals and alloys. Phys Rev B 1993;48:22–33.
[5] Cook RF, Pharr GM. Direct observation and analysis of indentation cracking in glasses and ceramics. J Am Ceram Soc 1990;73:787–817.
[6] Dolbow J, Gosz M. Effect of out-of-plane properties of a polyimide film on the stress fields in microelectronic structures. Mech Mater 1996;23:311–21.
[7] Dugdale DS. Yielding in steel sheets containing slits. J Mech Phys Solids 1960;8:100–4.
[8] Gao X-L, Jing XN, Subhash G. Two new expanding cavity models for indentation deformations of elastic strain-hardening materials. Int J Solids Struct 2006;43:2193–208.

[9] Gao X-L. An expanding cavity model incorporating strain-hardening and indentation size effects. Int J Solids Struct 2006;43:6615–29.
[10] Gerberich WW, Cordill MJ. Physics of Adhesion. Rep Prog Phys 2006;69:2157–203.
[11] Johnson KL. Contact mechanics. Cambridge: Cambridge University Press; 1985.
[12] Levinshtein ME, Rumyantsev SL, Shur M. Properties of advanced semiconductor materials (GaN, AlN, InN, BN, SiC, SiGe). John Wiley & Sons, Inc.; 2001.
[13] Marshall DB, Evans AG. Measurement of adherence of residually stressed thin films by indentation. I. Mechanics of interfacial delamination. J Appl Phys 1984;56:2632–8.
[14] Marshall DB, Evans AG. Measurement of adherence of residually stressed thin films by indentation. II. Experiments with ZnO/Si. J Appl Phys 1984;56:2639–44.
[15] Nguyen O, Repetto EA, Ortiz M, Radovitzky RA. A cohesive zone model of fatigue crack growth. Int J Fracture 2001;110:351–69.
[16] Ortiz M. Computational micromechanics. Comput Mech 1996;18:321–38.
[17] Rosenfeld LG, Ritter JE, Lardner TJ, Lin MR. Use of the microindentation technique for determining interfacial fracture energy. J Appl Phys 1990;67:3291–5.
[18] Ting TCT. Anisotropic elasticity. Oxford: Oxford University Press; 1996.
[19] Volinsky AA, Moody NR, Gerberich WW. Interfacial toughness measurements for thin films on substrates. Acta Mater 2002;50:441–66.
[20] Volinsky AA, Vella J, Adhihetty IS, Sarihan V, Mercado L, Yeung BH, et al. Microstructure and mechanical properties of electroplated Cu thin films. In: Mat Res Soc Symp Proc 649, 2000. p. Q5.3.
[21] Yang, B. A Boundary element methodology for crack path prediction in brittle materials incorporating the cohesive zone model. Dissertation. Houston: University of Houston; 1998.
[22] Yang B. Examination of free-edge delamination around an open hole in composite laminates. Int J Fract 2002;115:173–91.
[23] Yang B. A novel boundary-domain element method of initial stress, finite deformation and discrete cracks in multilayered anisotropic elastic solids. Int J Fract 2006;141:3–10.
[24] Yang B, Mall S, Ravi-Chandar K. A cohesive zone model of fatigue crack growth in quasibrittle materials. Int J Solids Struct 2001;38:3927–44.
[25] Yang B, Pan E. Efficient evaluation of three-dimensional Green's functions in anisotropic elastostatic multilayered composites. Engng Anal Bound Elem 2002;26:355–66.
[26] Yang B, Ravi-Chandar K. On the role of the process zone in dynamic fracture. J Mech Phys Solids 1996;44:1955–76.
[27] Yang B, Ravi-Chandar K. A single-domain dual-boundary-element formulation incorporating a cohesive zone model for elastostatic cracks. Int J Fract 1998;93:115–44.
[28] Yang B, Tewary VK. Efficient Green's function method of line and surface defects in multilayered elastic and piezoelectric materials. Comput Model Engng Sci 2006;15:165–78.
[29] Yang Q, Cox B. Cohesive models for damage evolution in laminated composites. Int J Fract 2005;133:107–37.
[30] Yuan FG, Yang S, Yang B. Three-dimensional Green's functions for composite laminates. Int J Solids Struct 2003;40:331–42.